The Supersymmetric Standard Models with Decaying and Stable Dark Matters

Xin Gao,[1] Zhaofeng Kang,[1] and Tianjun Li[1,2]

[1]*Key Laboratory of Frontiers in Theoretical Physics, Institute of Theoretical Physics, Chinese Academy of Sciences, Beijing 100190, P. R. China*

[2]*George P. and Cynthia W. Mitchell Institute for Fundamental Physics, Texas A&M University, College Station, TX 77843, USA*

(Dated: June 7, 2018)

Abstract

We propose two supersymmetric Standard Models (SMs) with decaying and stable dark matter (DM) particles. To explain the SM fermion masses and mixings and have a heavy decay DM particle S, we consider the Froggatt-Nielsen mechanism by introducing an anomalous $U(1)_X$ gauge symmetry. Around the string scale, the $U(1)_X$ gauge symmetry is broken down to a Z_2 symmetry under which S is odd while all the SM particles are even. S obtains a vacuum expectation value around the TeV scale, and then it can three-body decay dominantly to the second/third family of the SM leptons in Model I and to the first family of the SM leptons in Model II. Choosing a benchmark point in the constrained minimal supersymmetric SM with exact R parity, we show that the lightest neutralino DM is consistent with the CDMS II experiment. Considering S three-body decay and choosing suitable parameters, we show that the PAMELA and Fermi-LAT experiments and the PAMELA and ATIC experiments can be explained in Model I and Model II, respectively.

PACS numbers: 12.60.Jv, 14.70.Pw, 95.35.+d

I. INTRODUCTION

It is well known that supersymmetry privides an elegant solution to gauge hierarchy problem in the Standard Model (SM). In the Minimal Supersymmetric Standard Model (MSSM), gauge coupling unification can be realized, which give us the important hint of Grand Unified Theory (GUT). In addition, in the supersymmetric SMs, we can define a Z_2 symmetry called R parity under which the SM particles are even while their supersymmetric partners are odd. With R parity, we can avoid the dimension-four proton decay problem and evade the stringent constraints from the electroweak precision data naturally. Interestingly, the lightest supersymmetric particle (LSP) is stable due to the R parity, and then can be the dark matter (DM) candidate. For example, the lightest neutralino can be a viable cold DM candidate, which can give us the correct relic density as well.

During the last two years, there were quite a few very interesting DM experiments from indirect and direct dections. The ATIC [1] and PPB-BETS [2] collaborations have reported the measurements of cosmic ray (CR) electron/positron spectra at energies up to ~ 1 TeV. These data show an obvious excess over the expected background in the energy ranges $\sim 300 - 800\,\mathrm{GeV}$ and $\sim 500 - 800\,\mathrm{GeV}$, respectively. In the mean time, the PAMELA collaboration also released their first CR measurements of the positron fraction [3] and the $\bar{p}/p$ ratio [4]. Although the $\bar{p}/p$ ratio is consistent with the astrophysical expectation from the interactions between the CR nuclei and interstellar medium, the positron fraction indeed shows a significant excess for energies above $10\,\mathrm{GeV}$ up to $\sim 100\,\mathrm{GeV}$, compared to the background predicted by the conventional CR propagation models. Later, the Fermi-LAT collaboration has released data on the measurement of the electron/positron spectrum from 20 GeV to 1 TeV with unprecedented precision [5], and the HESS collaboration has released the data on the measurements of electron/positron spectrum from 340 GeV to 700 GeV [6], complementing their earlier measurements from 700 GeV to 5 TeV [7]. For simplicity, we will denote the Fermi-LAT collaboration as FERMI collaboration in the following. Although the corresponding data from the ATIC and the FERMI/HESS experiments are not fully consistent, it was shown that the DM models, where the DM particles annihilate or decay dominantly to the SM leptons, can explain these experiments by choosing the suitable DM particle mass and the proper final state particles.

To explain the PAMELA/ATIC experiments or the PAMELA/FERMI/HESS experiments from DM annihilations, we know that a large boost factor about 100-1000 is needed. However, from astrophysics, the N-body simulation shows that the boost factor from DM substructure can never be larger than 10 [8]. To solve this problem, one can consider the Sommerfield enhancement [9–11] or Breit-Wigner resonant enhancement [12]. Alternatively, we can also consider the non-thermal dark matter production so that the DM annihilation

cross section can be large [13]. In addition, if the DM particle is not absolutely stable and can decay dominantly to leptons, we can explain these experiments for the DM lifetime at the order $\tau \sim 10^{25} - 10^{27} s$ [14–18]. In particular, in the supersymmetric Standard Models, the LSP neutralino cannot explain the PAMELA/ATIC experiments or the PAMELA/FERMI/HESS experiments unless it can decay due to the suitable R-parity violation dimension-four operators. Furthermore, to fit the PAMELA and ATIC data via the Markov Chain Monte Carlo (MCMC) technique, one found that the DM mass is about 700 GeV for annihilation and 1.4 TeV for decay, and the favored final state is e^+e^- [19]. And to fit the PAMELA, FERMI, and HESS data, one found that the DM mass is about 2 TeV for annihilation and 4 TeV for decay, and the favored final states are the combination of $\mu^+\mu^-$ and $\tau^+\tau^-$ since the electron/positron spectra in the FERMI and HESS experiments are softer than these in the ATIC and PPB-BETS experiments [19]. Also, the HESS obervation of the Galactic center gamma rays gives strong constraint on the annihilation DM scenario while gives much weaker constraint on the decay DM scenario. Thus, it favors the decay DM [19].

Recently, the Cryogenic Dark Matter Search (CDMS) collaboration has observed two candidate DM events in the CDMS II experiment [20]. The recoil energies for these two events are 12.3 keV and 15.5 keV, respectively, and the data set an upper limit on the DM-nucleon elastic-scattering spin independent cross section around $10^{-8} - 10^{-7}$ pb. Because the probability of observing two or more background events is 23%, the CDMS II results cannot be a statistically significant evidence for DM interactions, but these two events can not be rejected as signal. In particular, the favored DM mass from the CDMS II data is about 100 GeV. Later, the CDMS II results have been studied extensively in various DM models [21]. Interestingly, the CDMS II experiment can be explained in the supersymmetric Standard Models where the LSP neutralino is DM.

In short, if the PAMELA, ATIC, FERMI, and HESS experiments indeed observed the DM annihilations or decays, the corresponding DM particle is heavy around a few TeVs. And if the two events observed by the CDMS II experiment are DM signals, the corresponding DM particle is light around 100 GeV. Therefore, there may exist at least two DM particles in the Nature. In fact, in almost all the previous DM models, the nearly universal implicit assumption is that there is one and only one DM particle. However, we cannot prove this implicit assumption, and then we cannot ingore the possibility of multicomponent DM [22, 23].

In this paper, we propose two supersymmetric Standard Models with decaying and stable DM particles. To avoid the proton decay problem and evade the stringent constraints from the electroweak precision data, we assume that R parity is not violated. In our models, we require that the LSP neutralino be the stable DM particle with mass around 100 GeV and the LSP neutralino-nucleon scattering cross section be about 10^{-8} pb. Thus, we can explain

the CDMS II experiment. We also assume that the supersymmetry breaking scale is still below 1 TeV, and then we can solve the gauge hierarchy problem without fine-tuning. To explain the PAMELA, ATIC, and FERMI experiments, we introduce a DM particle S with mass around a few TeVs. To produce the SM fermion masess and mixings and have the heavy decay DM particle S, we consider the Froggatt-Nielsen (FN) mechanism [24]. We introduce an anomalous $U(1)_X$ gauge symmetry whose anomaly is cancelled by the Green-Schwarz mechanism [25]. Especially, the $U(1)_X$ gauge symmetry is broken down to the Z_2 symmetry around the string scale under which S is odd while all the SM particles are even. Thus, S can be a DM particle. Similar to the discussions in Refs. [26–29], the SM fermion masses and mixings can be generated as well. With a pair of heavy vector-like particles that are SM singlets and have $U(1)_Y$ charges ± 1 respectively, we obtain that the leading Yukawa coupling terms between S and the SM particles are $S^2 H_d L_i E_j^c$ where H_d is the Higgs field, and L_i and E_j^c are the i-th family of the SM lepton doublet and j-th family of the right-handed charged lepton, respectively. In Model I, we have $(i,\ j) = (2,\ 2)$ and $(3,\ 2)$, while in Model II, we have $(i,\ j) = (1,\ 1)$. After S obtains a vacuum expectation value (VEV) at the TeV scale, S can decay dominantly to the second/third family of the SM leptons via dimension-six operators (three-body decay) in Model I, and to the first family of the SM leptons in Model II. To realize our idea, we present a benchmark point from the constrained minimal supersymmetric Stanard Model (CMSSM). The lightest neutralino $\widetilde{N}_1^0$ contributes to part of the whole DM relic density, *i.e.*, $\Omega_{\widetilde{N}_1^0} h^2 \approx 0.08$. The LSP neutralino-nucleon elastic-scattering spin independent cross section is about 5×10^{-9} pb. Thus, this benchmark point is consistent with the CDMS II results. In addition, for the S lifetime about $\tau \sim 10^{25} - 10^{27} s$, we can explain the PAMELA, FERMI and CDMS II experiments in Model I with S mass 3 TeV, and explain the PAMELA, ATIC and CDMS II experiments in Model II with S mass 1.8 TeV.

The paper is organized as follows. In Section II, we explain the SM fermion masses and mixings as well as the leading Yukawa terms $S^2 L_i H_d E_j^c$ via the FN mechanism. In Section III, we present a benchmark point in the CMSSM parameter space, and we discuss the DM particle S three-body cascade decay. We fit the PAMELA and FERMI data and the PAMELA and ATIC data in Section IV. Section V is our discussion and conclusions. We present more technical details in Appendices A, B, and C.

II. TWO SUPERSYMMETRIC STANDARD MODELS

In this Section, we will present two supersymmetric Standard Models with decaying and stable DM particles. To have a decay DM particle, we introduce a SM singlet field S and a new Z_2 symmetry. Under this Z_2 symmetry, S is odd while all the SM particles

are even. Thus, S can be a DM particle. Because the global discrete symmetry can be broken by the quantum gravity effects, it is natural to have the remnant discrete symmetry from an extra $U(1)'$ gauge symmetry [30, 31]. In particular, in the $U(1)'$-extended Minimal Supersymmetric Standard Model (UMSSM) [32] where we can solve the μ problem and avoid proton decay, we indeed have a new DM candidate if the $U(1)'$ is broken down to a Z_2 symmetry [23, 33].

In our models, this Z_2 symmetry is the residual symmetry after the anomalous $U(1)_X$ gauge symmetry breaking, *i.e.*, Z_2 is a subgroup of $U(1)_X$. After supersymmetry is broken at the TeV scale, the supersymmetry breaking soft masses may make m_S^2 negative and then the scalar component of S obtains a VEV around the TeV scale. We assume that the lightest state in the supermultiplet S is its scalar component, which is still denoted by S in this paper. In short, S is a DM particle which can decay after Z_2 symmetry breaking. In the concrete model building, we may need a singlet sector with additional particles and interactions for two kinds of reasons: (1) We have to stabilize the VEV of S at the TeV scale; (2) We need to generate the correct S relic density from thermal productions by considering the additional $U(1)'$ gauge symmetry at the TeV scale [23], or from non-thermal productions by considering the cosmic string at intermediate scale [13] or the extra vector-like particles at the intermediate scale [16]. Similar to the Ref. [16], we concentrate on the DM phenomenology in this paper, and then the detailed discussions of the singlet sector and S relic density are out of the scope of our current paper.

To explain the PAMELA, ATIC, FERMI and HESS experiments, S must decay dominantly to the SM leptons. To select the suitable final state particles, we consider the Froggatt-Nielsen mechanism [24], which is an elegant way to explain the SM fermion masses and mixings. We consider an anomalus $U(1)_X$ gauge symmetry, whose anomaly can be cancelled via the Green-Schwarz mechanism [25]. In the string model building, we indeed have at least one anomalous $U(1)_X$ gauge symmetry [29].

To break the $U(1)_X$ gauge symmetry, we introduce a flavon field A with $U(1)_X$ charge -1. Because supersymmetry must be preserved close to the string scale, A can acquire a VEV so that the $U(1)_X$ D-flatness can be realized. It was shown [27] that

$$0.171 \leq \epsilon \equiv \frac{\langle A \rangle}{M_{\rm Pl}} \leq 0.221 \ , \tag{1}$$

where $M_{\rm Pl}$ is the reduced Planck scale. Interestingly, ϵ is about the size of the Cabibbo angle. Let us explain our convention. We denote the SM left-handed quark doublets, right-handed up-type quarks, right-handed down-type quarks, left-handed lepton doublets, right-handed neutrinos, and right-handed charged leptons as Q_i, U_i^c, D_i^c, L_i, N_i^c, and E_i^c, respectively. Also, there is one pair of Higgs doublets H_u and H_d in the supersymmetric Standard Models. Moreover, we introduce a pair of vector-like particles E' and $\overline{E}'$ whose quantum numbers

under $SU(3)_C \times SU(2)_L \times U(1)_Y$ are $(\mathbf{1}, \mathbf{1}, -\mathbf{1})$ and $(\mathbf{1}, \mathbf{1}, \mathbf{1})$, respectively. In addition, the $U(1)_X$ charges for all the particles in our models are denoted by appropriate subscripts, for example, for a generic particle ϕ, its $U(1)_X$ charge is X_ϕ. In our models, we choose the $U(1)_X$ charges for the SM fermions and Higgs fields as follows

$$\begin{aligned} &X_{Q_1} = 3, \quad X_{Q_2} = 2, \quad X_{Q_3} = 0, \quad X_{U_1^c} = 5, \quad X_{U_2^c} = 2, \quad X_{U_3^c} = 0, \\ &X_{D_1^c} = 1, \quad X_{D_2^c} = 0, \quad X_{D_3^c} = 0, \quad X_{L_1} = 1, \quad X_{L_2} = 0, \quad X_{L_3} = 0, \\ &X_{E_1^c} = 3, \quad X_{E_2^c} = 2, \quad X_{E_3^c} = 0, \quad X_{H_u} = 0, \quad X_{H_d} = 0. \end{aligned} \tag{2}$$

The superpotential for the SM fermion Yukawa couplings is

$$\begin{aligned} W \supset &\left(\frac{A}{M_{\rm Pl}}\right)^{X_{H_u}+X_{Q_i}+X_{U_j^c}} Q_i H_u U_j^c + \left(\frac{A}{M_{\rm Pl}}\right)^{X_{H_d}+X_{Q_i}+X_{D_j^c}} Q_i H_d D_j^c \\ &+ \left(\frac{A}{M_{\rm Pl}}\right)^{X_{H_d}+X_{L_i}+X_{E_j^c}} L_i H_d E_j^c + \left(\frac{A}{M_{\rm Pl}}\right)^{X_{H_u}+X_{L_i}+X_{N_j^c}} L_i H_u N_j^c \ , \end{aligned} \tag{3}$$

where $i,\ j = 1,\ 2,\ 3$, and all the coefficients are assume to be order one in the above superpotential. Thus, we obtain the SM fermion Yukawa coupling matrixes Y_u, Y_d, Y_e and Y_ν respectively for up-type quarks, down-type quarks, charged leptons and active neutrinos

$$Y_u \sim \begin{pmatrix} \epsilon^8 & \epsilon^5 & \epsilon^3 \\ \epsilon^7 & \epsilon^4 & \epsilon^2 \\ \epsilon^5 & \epsilon^2 & 1 \end{pmatrix}, \quad Y_d \sim Y_e^T \sim \begin{pmatrix} \epsilon^5 & \epsilon^4 & \epsilon^4 \\ \epsilon^4 & \epsilon^3 & \epsilon^3 \\ \epsilon^2 & \epsilon^1 & \epsilon^1 \end{pmatrix}, \quad Y_\nu \sim \begin{pmatrix} \epsilon^2 & \epsilon & \epsilon \\ \epsilon & 1 & 1 \\ \epsilon & 1 & 1 \end{pmatrix} \ , \tag{4}$$

where T is transpose. We can show that the observed SM fermion masses and mixings can be generated [27, 29], and $\tan\beta = \langle H_u^0 \rangle / \langle H_d \rangle^0$ is 25.

In the Model I, we would like to explain the PAMELA and FERMI experiments. We choose the following $U(1)_X$ charges for S, E' and $\overline{E'}$

$$X_S = 3/2, \quad X_{E'} = -5, \quad X_{\overline{E}'} = 5. \tag{5}$$

Note that A has $U(1)_X$ charge -1, the $U(1)_X$ charges for the SM particles are integers, while the $U(1)_X$ charge for S is half integer, thus, the $U(1)_X$ gauge symmetry is broken down to a Z_2 symmetry after A obtains a VEV. In particular, under this Z_2 symmetry, only S is odd while all the other SM particles are even. Then the leading Yukawa coupling terms between S and the SM particles in the superpotential are

$$W \supset \left(\frac{A}{M_{\rm Pl}}\right)^5 H_d L_k \overline{E'} + \left(\frac{S^2}{M_{\rm Pl}}\right) E_2^c E' + M_V \overline{E'} E' \ , \tag{6}$$

where $k = 2,\ 3$, and M_V is the vector-like particle mass around the 10^{13} GeV. In particular, the superpotential mass terms $E_i^c E'$ and $A^n E_i^c E'$ are forbidden due to the holomorpic

property of superpotential. Because E' and $\overline{E'}$ are heavy, we should integrate them out below their mass scale. From the above superpotential, we obtain from equations of motion (EOMs) for E' and $\overline{E'}$

$$E' \;=\; -\frac{H_d L_k}{M_V}\;, \quad \overline{E'} \;=\; -\frac{S^2 E_2^c}{M_V M_{\rm Pl}}\;. \tag{7}$$

Using the above EOMs for E' and $\overline{E'}$, we obtain that the superpotential in Eq. (6) becomes

$$W \supset \; -\epsilon^5 \left(\frac{S^2}{M_{\rm Pl} M_V}\right) H_d L_k E_2^c\;. \tag{8}$$

To simplify the discussions, we assume that the coefficient of $S^2 H_d L_2 E_2^c$ is about three times larger than that of $S^2 H_d L_3 E_2^c$. Thus, we will concentrate on the term $S^2 H_d L_2 E_2^c$ in the following discussions.

In the Model II, we want to explain the PAMELA and ATIC experiments. We choose the $U(1)_X$ charges for S, E' and $\overline{E'}$ as follows

$$X_S = 1/2, \quad X_{E'} = -4, \quad X_{\overline{E}'} = 4. \tag{9}$$

Similar to the Model I, the $U(1)_X$ gauge symmetry is broken down to a Z_2 symmetry after A obtains a VEV. Under this Z_2 symmetry, only S is odd while all the other SM particles are even. Then the leading Yukawa coupling terms between S and the SM particles in the superpotential are

$$W \supset \left(\frac{A}{M_{\rm Pl}}\right)^4 H_d L_1 \overline{E'} + \left(\frac{S^2}{M_{\rm Pl}}\right) E_1^c E' + M_V \overline{E'} E'\;. \tag{10}$$

Similar to the Model I, integrating out the vector-like particles $\overline{E'}$ and E', we obtain

$$W \supset \; -\epsilon^4 \left(\frac{S^2}{M_{\rm Pl} M_V}\right) H_d L_1 E_1^c\;. \tag{11}$$

In this paper, we will define $M_*^2 = M_{\rm Pl} M_V/\epsilon^n$ where n is equal to 5 in Model I and 4 in Model II. With M_V around 10^{13} GeV, we obtain that M_* is around 10^{17} GeV. To get M_V around 10^{13} GeV, we can introduce additional global $U(1)''$ symmetry and a SM singlet field S' which breaks the $U(1)''$ symmetry. The $U(1)''$ charges for L_i, E_i^c, $\overline{E'}$, S, and S' are 1, -1, -1, 1/2 and 1, while the $U(1)''$ charges for all the other particles are zero. Therefore, all the previous terms in the superpotential including the SM fermion Yukawa coupling terms are invariant except the term $M_V \overline{E'} E'$. The vector-like mass term for $\overline{E'}$ and E' can be generated by the following superpotential term after the $U(1)''$ symmetry breaking

$$W \;\supset\; S' \overline{E'} E'\;. \tag{12}$$

Assuming that S' acquires a VEV around 10^{13} GeV, we obtain that M_V is around 10^{13} GeV.

By the way, the other Yukawa coupling terms among S, the SM fermions and Higgs fields might have the prefactor $\left(\frac{S^2}{M_{\rm Pl}^2}\right)^n \left(\frac{A}{M_{\rm Pl}}\right)^m (...)$ ($n \geq 1$ or $m \geq 1$). Thus, these Yukawa coupling terms are supressed by at least the Planck scale square and then are negligible since S's VEV is around the TeV scale. In this paper, we only consider the minimal Kähler potential. In general, the dimension-six operators of the form $SS^\dagger\phi\phi^\dagger/M_{\rm Pl}^2$ cannot be forbidden by any symmetry where ϕ denotes the SM fermions and Higgs fields. These dimension-six operators can induce DM two-body decay through derivative couplings [16]. However, their contributions to the CR are also ignorable since these operators are suppressed by the Planck scale square as well.

III. DECAY AND STABLE DARK MATTERS

A. The CMSSM Benchmark Point for CDMS II Experiment

The CMSSM with the LSP neutralino as DM has been studied extensively before. Typically, the LSP neutralino with mass about tens of GeV is in tension with the lightest CP-even Higgs boson mass whose low bound from the LEP is 114 GeV. Especially, we require that the LSP neutralino relic density be small about half of the total DM relic density, *i.e.* $\Omega_{\widetilde{N}_1^0}h^2 \sim 0.06$. In this paper, we do not scan all the viable parameter space. We only consider a CMSSM benchmark point that satisfies all the constraints. We choose the following five free parameters at the GUT scale

$$m_0 = 310\text{GeV}, \quad m_{1/2} = 250\text{GeV}, \quad A_0 = -1040, \quad \tan\beta = 30, \quad \text{sign}(\mu) = +1. \tag{13}$$

As expected, this benchmark point is in the coannihilation region [34] with small mass difference between the light stau $\widetilde{\tau}_1$ and LSP neutralino, *i.e.*, $m_{\widetilde{\tau}_1} - m_{\widetilde{N}_1^0} \leq 8$ GeV. Such benchmark point is not interesting previously since the LSP neutralino relic density is smaller than the observed whole DM relic density. However, it is fine in our models since we have two DM particles. With MicrOMEGAs 2.0 [35], we obtain the LSP neutralino relic density

$$\Omega_{\widetilde{N}_1^0}h^2 \approx 0.08\ . \tag{14}$$

Moreover, the mass of the LSP neutralino is about 101.6 GeV. And the spin-independent cross section between the LSP neutralino and nucleon is about $\sigma_{SI} \approx 5\times10^{-9}$ pb. Although this cross section is a little bit small, we can still explain the CDMS II experiment due to the uncertainties of the QCD effects in the calculations.

It is necessary to address the mass spectrum of this benchmark point in details for the following calculations. The lightest neutralino $\widetilde{N}_1$ is bino-like, while the heavy neutralinos

$\widetilde{N}_{3,4}$ are Higgsino-like. Since $\tan\beta$ is large, in the charged Higgs boson system, H_u^+ is the major component of the Goldstone boson, with the ratio to $(H_d^-)^*$ to be $\tan^2\beta : 1$. So we can treat H_d^- as the charged Higgs boson C^- approximately, *i.e.*, $H_d^- \approx C^-$. The CP-odd neutral Higgs and charged Higgs mass matries are diagonlized by the same matrix. Thus, the imaginary part of H_u^0 gives the main component of the Goldstone boson, while A^0 is mainly the imaginary part of H_d^0, *i.e.*, $A^0 \approx \mathrm{Im}(H_d^0)$. Same conclusion applies to the heavy CP-even Higgs boson H^0, *i.e.*, $H^0 \approx \mathrm{Re}(H_d^0)$ because H^0 is equal to $\cos\alpha \mathrm{Re}(H_d^0) + \sin\alpha \mathrm{Re}(H_u^0)$ with $\alpha \approx -0.04$. As for the chargino system, the large μ term implies that the charged Higgsino is the major component of heavy chargino $\widetilde{C}_2^-$. Because we need to use the neutralino, chargino and Higgs mixing matrices in the following discussions, we calculate the relevant masses and mixings at low energy by SuSpect [36]. For the neutralino system, the four particles $(-i\widetilde{B}, -i\widetilde{W}_3, \widetilde{H}_d^0, \widetilde{H}_u^0)$ are transformed into the mass eigenstates $(\widetilde{N}_1^0, \widetilde{N}_2^0, \widetilde{N}_3^0, \widetilde{N}_4^0)$ by the unitary matrix Z

$$\begin{pmatrix} -i\widetilde{B} \\ -i\widetilde{W}_3 \\ \widetilde{H}_d^0 \\ \widetilde{H}_u^0 \end{pmatrix} = \begin{pmatrix} 1.00 & -0.02 & 0.08 & -0.02 \\ 0.03 & 0.99 & -0.16 & 0.06 \\ 0.04 & -0.07 & -0.70 & -0.71 \\ 0.07 & -0.15 & -0.69 & 0.70 \end{pmatrix} \begin{pmatrix} \widetilde{N}_1^0 \\ \widetilde{N}_2^0 \\ \widetilde{N}_3^0 \\ \widetilde{N}_4^0 \end{pmatrix}. \tag{15}$$

And the neutralino mass eigenvalues are $m_{\widetilde{N}_{1,2,3,4}} = 101.6,\ 196.2,\ 571.0,\ 577.0$ GeV, respectively. The particles $(W_3^-,\ H_d^-)$ and $(\mathrm{Re}(H_d^0),\ \mathrm{Re}(H_u^0))$ can be written respectively in terms of their mass eigenstates as follows

$$\begin{pmatrix} \widetilde{W}_3^- \\ \widetilde{H}_d^- \end{pmatrix} = \begin{pmatrix} -0.98 & 0.22 \\ 0.22 & 0.98 \end{pmatrix} \begin{pmatrix} \widetilde{C}_1^- \\ \widetilde{C}_2^- \end{pmatrix}, \quad \begin{pmatrix} \mathrm{Re}(H_d^0) \\ \mathrm{Re}(H_u^0) \end{pmatrix} = \begin{pmatrix} 1.00 & 0.04 \\ -0.04 & 1.00 \end{pmatrix} \begin{pmatrix} H^0 \\ h^0 \end{pmatrix}, \tag{16}$$

with $m_{\widetilde{C}_{1,2}^-} = 196.1,\ 578.5$ GeV, and $m_{h^0,H^0} = 117.90,\ 510.81$ GeV. The $\mathrm{Im}(H_d^0)$ and $\mathrm{Im}(H_u^0)$ are not given explicitly here, and the mass of the CP-odd Higgs field A^0 is 512.49 GeV.

B. DM S Three-Body Decays

In this paper, we will concentrate on the calculations in Model I. For simplicity, we will not explain the calculations in Model II since the calculations are not only similar but also simpler. To analyze the DM S primary decays, we write the operator in the components explicitly

$$\begin{aligned} \mathcal{C}_\mu S H_d L E^c + c.c. &= \mathcal{C}_\mu S H_d^0 E E^c - \mathcal{C}_\mu S H_d^- \nu E^c + c.c. \\ &\supset \mathcal{C}_\mu S(H_d^0 \mu_L \mu_R^\dagger + \widetilde{H}_d^0 \mu_L \widetilde{\mu}_R^* + \widetilde{H}_d^0 \widetilde{\mu}_L \mu_R^\dagger) - \mathcal{C}_\mu S(H_d^- \nu_\mu \mu_R^\dagger + \widetilde{H}_d^- \nu_\mu \widetilde{\mu}_R^* + \widetilde{H}_d^- \widetilde{\nu}_\mu \mu_R^\dagger) \\ &\quad + \mathcal{C}_\mu \widetilde{S}(H_d^0 \mu_L \widetilde{\mu}_R^* + H_d^0 \widetilde{\mu}_L \mu_R^* + \widetilde{H}_d^0 \widetilde{\mu}_L \widetilde{\mu}_R^* + \widetilde{H}_d^0 \widetilde{\mu}_L \widetilde{\mu}_R^\dagger) \\ &\quad - \mathcal{C}_\mu \widetilde{S}(H_d^- \nu_\mu \widetilde{\mu}_R^* + H_d^- \widetilde{\nu}_\mu \mu_R^* + \widetilde{H}_d^- \widetilde{\nu}_\mu \widetilde{\mu}_R^* + \widetilde{H}_d^- \widetilde{\nu}_\mu \widetilde{\mu}_R^\dagger), \end{aligned} \tag{17}$$

where $\mathcal{C}_\mu$ is equal to $\langle S\rangle/M_*^2$ times the order one coefficient. If these states are transferred to the mass eigenstates, further mixing factor must be included. After H_d^0 obtains a VEV, we shall have two-body and three-body S decays. Comparing to the two-body S decays, the three-body S decays have an extra factor $(M_D/\langle H_d^0\rangle)^2/(96\pi^2)$ where m_D is the mass of the heavy DM particle S. In our models, we choose $M_D = 3$ TeV and $\tan\beta = 30$, and then we get $(M_D/\langle H_d^0\rangle)^2/(96\pi^2) \sim 282$, Therefore, we only consider three-body S decays in this paper.

The heavy decay DM particle is the scalar component of S, whose three-body on-shell decays are given by the second line of Eq. (17)

$$S \to \widetilde{N}_{3,4}\mu\widetilde{\mu}_R, \quad \widetilde{C}_{1,2}\nu_\mu\widetilde{\mu}_L, \quad \widetilde{C}_{1,2}\mu\widetilde{\nu_\mu}_L, \quad A^0(H^0)\mu\mu, \quad C^-\nu_\mu\mu_R\ . \tag{18}$$

With the Eq. (B9) in the Appendix B, we obtain that all these nine primary decay channels almost have the democratic rates except the mixing factor for each channel. Anyway, the total decay rate is given by

$$\Gamma_{total} = \frac{1}{128\pi^3}\frac{\langle S\rangle^2 m_D^2}{M_*^4}\left(\sum_I \mathcal{C}_I^2 R_I\right) \times m_D, \tag{19}$$

where I denotes the I-th decay channel in Eq. (18). In our paper, the DM particle S is so heavy that the phase space suppressing factor R_I is almost process independent and is a constant around 1/6 (see Eq. (B9)). Then, the scale of the DM S lifetime is estimated to be

$$\tau_S \sim 2.7\times 10^{26} \times \left(\frac{3\text{TeV}}{m_D}\right)^3 \left(\frac{M_*}{10^{17}\text{GeV}}\right)^4 \left(\frac{3\,\text{TeV}}{\langle S\rangle}\right)^2 \left(\frac{1}{\sum_I \mathcal{C}_I^2 R_I}\right) s. \tag{20}$$

The random coefficient of the operator has been set to be 1. Notice that except the last factor, Eq. (20) is the so-called τ_{eff} which is the inverse of Γ_{eff} defined in Eq. (B9).

IV. COSMIC RAY ANOMALIES

Although the very large astrophysical uncertainties do exist in the calculations of cosmic ray, we do not want to scan all the viable parameter space. We only want to demonstrate that with appropriate parameters, we can explain the PAMELA and FERMI experiments in Model I and explain the PAMELA and ATIC experiments in Model II.

A. Cosmic $e^\pm$ Excess

In the Micky Way dark halo, the DM S decays into the SM particles, which propagate to the solar system. The propogation of charged particles is described by diffusion equation.

For instance, the diffusion equation for positron is

$$\frac{\partial \psi}{\partial t} - \nabla \cdot (K(\vec{x}, E)\nabla\psi) - \frac{\partial}{\partial E}\left(b(E)\psi\right) = q(\vec{x}, E), \tag{21}$$

where $\psi(\vec{x}, E)$ denotes the positron number density per unit energy. Diffusion coefficient $K = K_0 E^\delta$ is space independent. The third term describes the energy loss of positron through the synchrotron radiation and inverse Compton scattering, with loss ratio $b(E) = E^2/\tau_E$ where $\tau_E = 10^{16}s$. $q(\vec{x}, E)$ is the positron source term, describing the positron number density injected at $\vec{x}$, per unit time and energy. For simplicity, it can be expressed as the product of an astrophysics factor and a particle physics factor

$$q(\vec{x}, E) = \left(\frac{1}{\tau_S}\sum_{I,F}\frac{dN^e_{I,F}}{dE}B_{I,F}\right) \times \frac{\rho(\vec{x})}{m_D}, \tag{22}$$

where we introduce another index F to distinguish the different states from the I-th decay channel. Moreover, the Milky Way DM density profile $\rho(\vec{x})$ in the spherical coordinates is generically written as

$$\rho(r) = \rho_\odot \left(\frac{r_\odot}{r}\right)^\gamma \left(\frac{1 + (r_\odot/r_s)^\alpha}{1 + (r/r_s)^\alpha}\right)^{(\beta-\gamma)/\alpha}, \tag{23}$$

where $r_\odot = 8.5$ kpc is the distance from the solar system to the Milky Way center, and the DM profile density in the solar system is set to be $\rho_\odot = 0.3\,\mathrm{GeV\,cm^{-3}}$. According to the $N-$body simulation, it has three popular choices parameterized by (α, β, γ). We use the NFW profile with $(1, 3, 1)$ [37], and choose the DM central core $r_s = 20$ kpc. By the way, the injected source term is linearly proportional to the decay DM relic density. Therefore, the fraction of the DM S relic density r_{DM} to the whole DM relic density should be taken into account. For simplicity, we absorb it into the redefinition of S lifetime by $\tau_S \to r_{DM}\tau_S$ without disturbing any other terms.

The normalized energy spectrum distribution function $dN^e_{I,F}/dE = (2/m_D)dN^e_{I,F}/dx$ describes the positrons from the specific DM decay intermediate state (I, F), with $(I, F) = \widetilde{\mu}_L$, A^0..., and so on. And $B_{I,F} = B_I$ is the corresponding branch ratio. In this paper, summing over all the channels (see Appendix, with a little bit changed notation), we obtain the total fragmentation function

$$\frac{dN^S_e}{dx} = \frac{\Gamma_{eff}}{\Gamma_{total}}\sum_{I,F}\left(\mathcal{C}^2_{I,F}R_{I,F}\right) \times \frac{1}{R_{I,F}}\frac{d\widetilde{N}}{dx_{I,F}} \otimes \frac{dN}{dx_e^{I,F}}, \tag{24}$$

where $dN/dx_{I,F}$ and $1/R_{I,F}dN/dx_e^{I,F}$ respectively give the fragmentation functions in the rest frame of the DM S and particle (I, F). The former is analytically calculable, while the later is obtained through PYTHIA [38] simulation (except for muon decay, we shall use the

analytical formula). The total spectrum is their convolution, whose explicit form can be found in Eq. (B12). By the way, when we put Eq. (24) into Eq. (22), the τ_S factor in the front of source term in Eq. (22) is cancelled by factor Γ_{total} in Eq. (24). So, τ_{eff} or Γ_{eff} is still the free parameter in the calculations of positron propagation.

Eq. (21) can be approximately solved analytically. The final positron flux observed at the Earth $\Phi_{e^+}(r_\odot, E)$ is factorized into the convolution of $\mathcal{H}_e(E_s, E)$ which encodes the whole astrophysical information and the inject spectrum dN_S^e/dE_s

$$\Phi_{e^+}(r_\odot, E) = \frac{\beta_{e^+}}{4\pi}\kappa\frac{\tau_E}{E^2}\int_E^{E_{max}} \mathcal{H}_e(E_s, E)dE_s\frac{dN_S^e}{dE_s} \ , \tag{25}$$

where β_{e^+} is the velocity of the observed positron and $\kappa = \rho_\odot/(\tau_{eff}\, m_D)$. The concrete method to calculate the halo functions for electron $\mathcal{H}_e(E_s, E)$ and for anti-proton $\mathcal{H}_{\bar{p}}(E)$ can be found in Ref. [8, 39].

To compare the data, we should consider the cosmic background. It is believed that the astrophysical $e^\pm$ source is mainly due to supernova explosions (primary e^-) and the interactions between the CR nuclei and light atoms in interstellar medium (secondary $e^\pm$). They are usually parameterized in the following form [40]

$$\begin{aligned}
\Phi_{e^-}^{bk,pri} =& \frac{0.16E^{-1.1}}{1+11E^{0.9}+3.2E^{2.15}}, \quad \Phi_{e^-}^{bk,sec} = \frac{0.7E^{0.7}}{1+110E^{1.5}+600E^{2.9}+580E^{4.2}}, \\
\Phi_{e^+}^{bk,sec} =& \frac{4.5E^{0.7}}{1+650E^{2.3}+1500E^{4.2}},
\end{aligned} \tag{26}$$

where the unit is $\mathrm{GeV}^{-1}\mathrm{cm}^{-2}s^{-1}sr^{-1}$. $\Phi_{e^-}^{bk,pri}$, $\Phi_{e^-}^{bk,sec}$, and $\Phi_{e^+}^{bk,sec}$ are the background fluxes for the primary electron, secondary electron, and secondary positron, respectively. Then the positron fraction observed by the PAMELA experiment and the normalized total electron/positron fluxes observed by the FERMI and ATIC experiments are respectively given by

$$\begin{aligned}
\frac{\Phi_{e^+}}{\Phi_{e^+}+\Phi_{e^-}} &= \frac{\Phi_{e^+}^{bk,sec}+\Phi_{e^+}^{DM}}{\kappa\Phi_{e^-}^{bk,pri}+\Phi_{e^+}^{bk,sec}+\Phi_{e^-}^{bk,sec}+\Phi_{e^+}^{DM}+\Phi_{e^-}^{DM}} \ , \\
E_e^3(\Phi_{e^+}+\Phi_{e^-}) &= E_e^3(\kappa\Phi_{e^-}^{bk,pri}+\Phi_{e^+}^{bk,sec}+\Phi_{e^-}^{bk,sec}+\Phi_{e^+}^{DM}+\Phi_{e^-}^{DM}) \ ,
\end{aligned} \tag{27}$$

where $\kappa \leq 1$ is a parameter which includes the uncertainties of the primary background electron production.

The PAMELA positron fraction data and FERMI electron/positron data can be fitted very well by choosing proper τ_{eff} and κ. The primary DM S three-body decays into muons, which subsequently decay to electron/positron, give the hard positron energy spectrum that is necessary to explain the steep rise in positron fraction observed by the PAMELA experiment [17]. As for the FERMI experiment, its data show a rather flat spectrum up to

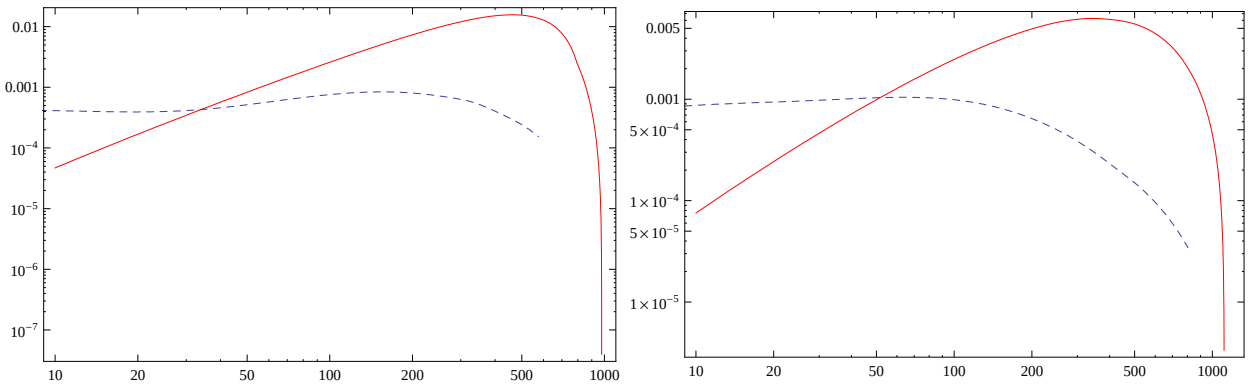

FIG. 1: The comparison between the contributions to total $e^{\pm}$ fluxes from μ in Model I (or e in Model II) and all the other particle cascade decays. The red line denotes the contribution from μ (or e), while the dashed line denotes the contributions from the other particles. The left figure is for Model II with $m_D = 1.8$ TeV, and the right figure for Model I with $m_D = 3.0$ TeV.

about 1 TeV. Moreover, there are a faint minimum and a faint peak at about 100 GeV and 400 GeV, respectively, which can be considered as the subtle fine structure. Interestingly, we can fit such structure as well. The possible reason is that: at low energy ($\lesssim 50$ GeV), the DM S decay contributions to the observed electron/positron spectrum are dominated by these from A^0, H^0... channels; while at high energy, they are dominated by these from cascade muon decays. The muon decays produce a relative harder spectrum, which is peaked around 400 GeV. Because the peak varies with the DM particle mass, this explains why we choose $m_D = 3$ TeV as a typical fitting value in Model I. In Fig. 1, we compare these two contributions in Model I with $m_D = 3.0$ TeV and in Model II with $m_D = 1.8$ TeV. In Fig. 2, we present the fitting for the FERMI data in Model I with $\tau_{eff} = 0.72 \times 10^{26} s$, $m_D = 3.0$ TeV, and $\kappa = 0.65$, and the fitting for the ATIC data in Model II with $\tau_{eff} = 0.52 \times 10^{26} s$, $m_D = 1.8$ TeV and $\kappa = 0.67$. In short, these fittings are pretty good especially at relative low energy.

In addition, from Fig. 3, we obtain that our fitting for the PAMELA positron fraction data in Model II looks fine since the positron spectrum from the DM direct three-body decay is relatively harder. However, we can not fit the PAMELA positron fraction data in Model I very well in the low energy region (< 20 GeV). The reason is that the low energy positron data are dominated by the sparticle and Higgs boson cascade decays, which produce large number of soft electron/positron. Therefore, the positron fraction can exceed the background value. Interestingly, the main character at the high energy region is reproduced pretty well. Especially, the steep rising is obvious due to the harder positrons from muon

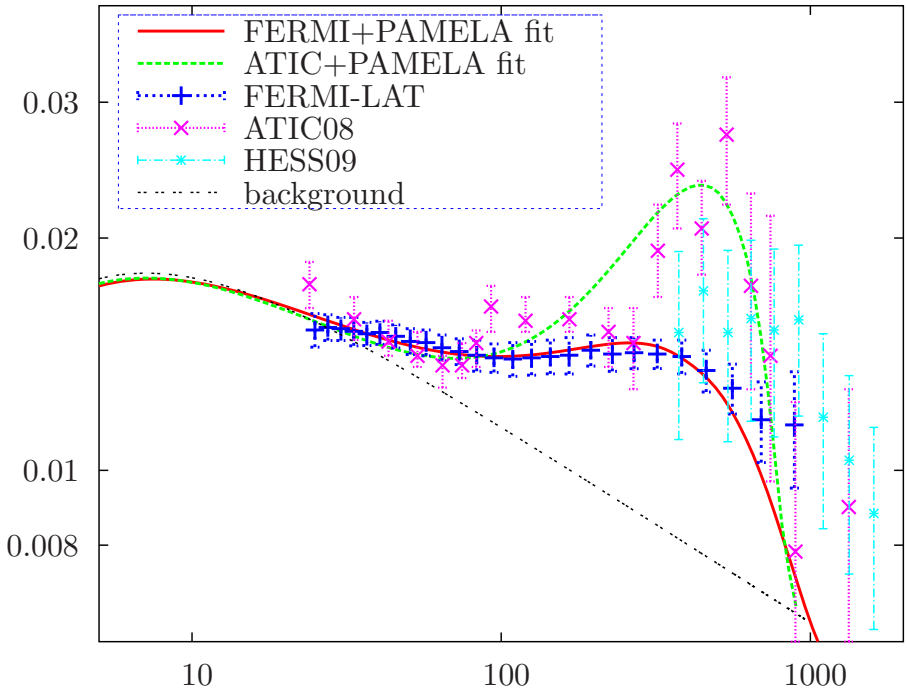

FIG. 2: The FERMI data fitting in Model I and the ATIC data fitting in Model II.

decay. Moreover, it predicts a continuously going up trend until arriving at the peak around 0.5 TeV, which can be tested by the upcoming PAMELA experiment.

B. Anti-Proton Fluxes

Bcause Higgs bosons and charginos can couple to the SM quarks, their decays may produce anti-proton excess as well. However, the anti-proton excess is not observed by the PAMELA experiment. The propagation of anti-proton is similar to that of positron, but it is simpler by the virtue of no energy loss process from the inverse Compton scattering

$$\frac{\partial\psi}{\partial t} - \nabla\cdot(K(\vec{x},E)\nabla\psi) + \nabla\cdot(\vec{V}_c(\vec{x})\psi) = q(\vec{x},E) - 2h\delta(z)\Gamma_{ann}\psi \ . \tag{28}$$

However, the Milky Way's galactic wind $\vec{V}_c(\vec{x})$, which is usually assumed along the z axial direction and then is reduced to $V_c\,\mathrm{sign}(z)\vec{k}$, induces the drift of anti-protons during propagation, as reflected in the third term. The last term represents the annihilations between the anti-protons and interstellar protons in the galactic plane, whose thickness is about $h \approx 0.1$ kpc $\ll L$, the half-thickness of cylinder diffusion region of charged particles. The

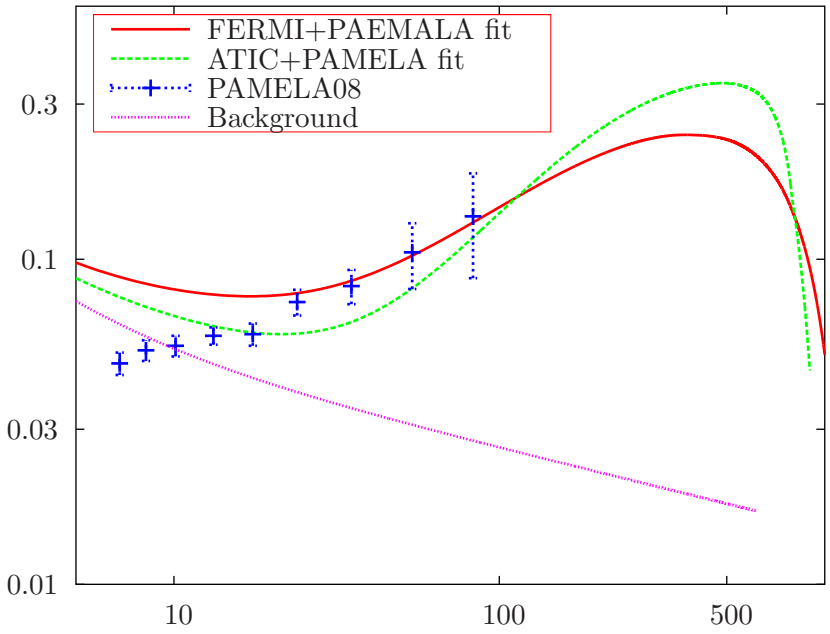

FIG. 3: PAMELA data fitting for positron fraction in Model I and Model II.

annihilation rate is given by $\Gamma_{ann} = (n_H + 4^{2/3} n_{He}) \sigma^{ann}_{p\bar{p}} v_{\bar{p}}$ with [41]

$$\sigma^{ann}_{p\bar{p}} = \begin{cases} 661(1 + 0.0115T^{-0.774} - 0.984T^{0.0151})\text{mbarn}, & \text{for } T < 15.5\,\text{GeV} \\ 36T^{-0.5}\text{mbarn}, & \text{for } T \geq 15.5\text{GeV} \end{cases} , \tag{29}$$

where $T = E - m_p$ is the proton kinetic energy. We can use K_0, δ, V_c and L to classify the astrophysical models that are compatible with the B/C ratio into three types [8], where K_0 and δ appear in the diffusion coefficient K. And each type is characterized by the flux of anti-protons. To suppress the anti-proton flux, we choose the parameters which can produce the minimal anti-protons: $\delta = 0.85$, $K_0 = 0.0016$ kpc^{2}Myr^{-1}, L=1 kpc, and $V_c = 13.5$ km s^{-1}.

Similarly, the anti-proton flux at the heliosphere boundary is formally solved to be

$$\Phi^{\bar{p}}_{\odot}(E) = \frac{1}{\Gamma_{total}} \times \frac{\beta_{\bar{p}}}{4\pi} \times \frac{dN^S_{\bar{p}}}{dE} \times \mathcal{H}_{\bar{p}}(E) , \tag{30}$$

where

$$\frac{dN^S_{\bar{p}}}{dx} = \frac{\Gamma_{eff}}{\Gamma_{total}} \sum_{I,F} \left(\mathcal{C}^2_{I,F} R_{I,F}\right) \times \frac{1}{R_{I,F}} \frac{d\widetilde{N}}{dx_{I,F}} \otimes \frac{dN}{dx^{I,F}_p} . \tag{31}$$

For details, please see Appendix B.

It is much simpler to obtain the flux for anti-proton than that of positron. The point is that the astrophysical information is totally factorized out in $\mathcal{H}_{\bar{p}}(E)$, and no further convolution operation is needed. The predicted anti-proton fluxes comparing to the background flux in Model I and Model II are plotted in Fig. 4, where the suitable astrophysical parameters have been chosen. The background anti-protons mainly arise from the collisions between the primary CR protons (produced also by supernova) and the interstellar hydrogen gas (for details, please see Ref. [41]). Taking proper astrophysics parameters in the practical calculations, we find that the anti-proton excess is definitely excluded below 50 GeV (Sixteen of the PAMELA seventeen points on $\bar{p}/p$ are in this energy region [3].). In Model I for the PAMELA and FERMI data fitting, the DM particle S is very heavy about 3 TeV, and then the anti-proton flux is suppressed in all energy region below about 130 GeV. However, in Model II for the PAMELA and ATIC data fitting, the DM particle S is about 1.8 TeV, and then the anti-proton flux begins to exceed background above about 60 GeV. Especially, the excess is more significant as the energy increasing, which is interesting since it can be tested in the future.

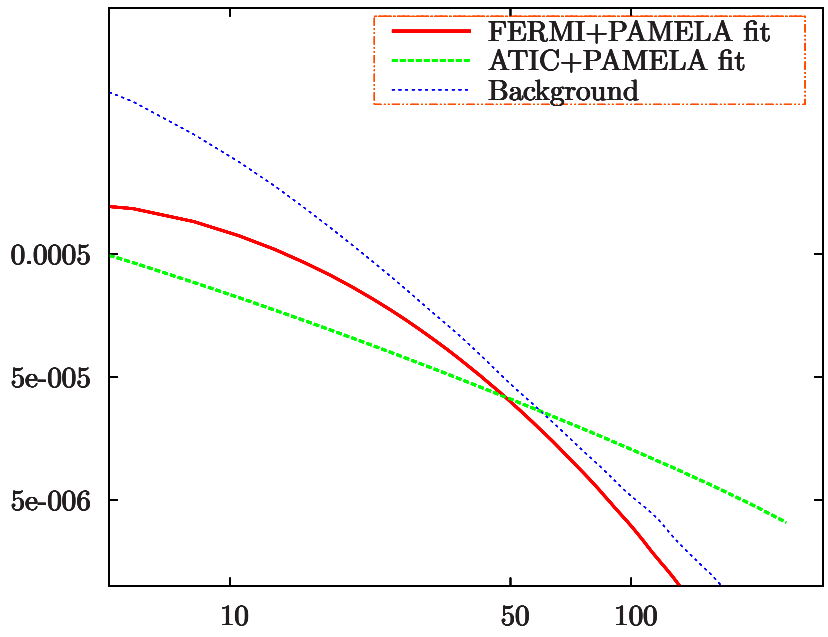

FIG. 4: PAMELA data fitting for $\bar{p}/p$ ratio in Model I and Model II. The anti-proton fluxes $\Phi_{\odot}^{\bar{p}}(E)$ is in the unit $\mathrm{GeV}^{-1}\mathrm{m}^{-2}\mathrm{s}^{-1}\mathrm{sr}^{-1}$.

V. DISCUSSION AND CONCLUSIONS

We proposed two supersymmetric Standard Models with decaying and stable DM particles. To explain the SM fermion masses and mixings, we considered an anomalous $U(1)_X$ gauge symmetry whose anomaly is cancelled by the Green-Schwarz mechanism. Around the string scale, the $U(1)_X$ gauge symmetry is broken down to the Z_2 symmetry under which only S is odd. Thus, S is stable and can be a DM candidate. After S obtains a VEV around the TeV scale, the Z_2 symmetry is broken and then S can decay. In our models, on the one hand, the LSP neutralino has mass 101.6 GeV, and its relic density is about $\Omega_{\widetilde{N}_1^0}h^2 \approx 0.08$. Because the lightest neutralino-nucleon cross section is 5×10^{-9} pb, the CDMS II results can be explained. On the other hand, S is a decay DM particle that can three-body cascade decay into the MSSM particles. With suitable $U(1)_X$ charges, S decays dominated into the second family of the SM leptons in Model I and into the first family of the SM leptons in Model II. In Model I, if the mass of the DM particle S is 3 TeV and S has effective lifetime about $\tau_{eff} \approx 0.72 \times 10^{26}s$ (the real lifetime is about $2.2 \times 10^{26}s$), we are able to explain the PAMELA/FERMI experiments simultaneously. In Model II, if the mass of the DM particle S is 1.8 TeV and S has effective lifetime about $\tau_{eff} \approx 0.52 \times 10^{26}s$, we can explain the PAMELA/ATIC experiments as well. In addition, taking the proper astrophysics parameters that produce the minimal anti-protons, we have shown that our models are consistent with $\bar{p}/p$ measurement in the PAMELA experiment.

Finally, although the accompanied gamma-ray and neutrino fluxes are not discussed here, they deserve further study. The primary hard neutrinos, as well as the soft gammas and neutrinos during the sparticle and Higgs fragmentations are produced. They may provide the spectrum properties through the inverse Compton scattering [42] that can be tested by the ongoing FERMI experiment. In addition, the complete and systematic studies of the multi-body decays and multi-contributions are interesting since we do need them in the DM model building. Furthermore, it is interesting to study the CMSSM parameter space where the LSP neutralino relic density is smaller than the observed total DM relic desity since we may have multicomponent DM.

Acknowledgments

We would like to thank Xiao-Jun Bi, Xian Gao, Wan-Lei Guo, Chun-Li Tong, Peng-fei Yin, Qiang Yuan, and Xinmin Zhang for helpful discussions. This research was supported in part by the Natural Science Foundation of China under grant No. 10821504, by the DOE grant DE-FG03-95-Er-40917 (TL), and by the Mitchell-Heep Chair in High Energy Physics (TL).

Appendix A: The DM S Three-body Decay

In this Appendix, we develop some useful approximation formulae for the three-body DM S decay. First, let us explain the convention. The decay width is calculated in the rest frame of the heavy parent particle S (Fermionic or scalar component depends on the choice.). In a decay channel, we always have the order of the final state masses as $m_3 > m_2 > m_1$.

In this case, in general m_3 is the mass of a slepton or Higgs bonson, with $m_3/m_D \lesssim 0.1$. And m_2 denotes the mass of Higgsino, $m_2/m_D \lesssim 0.05$. Finally, the lightest particle is either muon or neutrino, whose mass $m_1 = m_{\mu,\nu} < 10^{-4} m_D$ is ignorable. To simplify the calculations we set $m_1 = 0$.

First, we consider a general three-body decay process described by a heavy complex scalar S with mass M that decays into two fermions $\psi_{1,2}$ plus a scalar ϕ_3. The Feynman diagram is given in Fig. 5. It is not difficult to get the corresponding amplitude square with the final

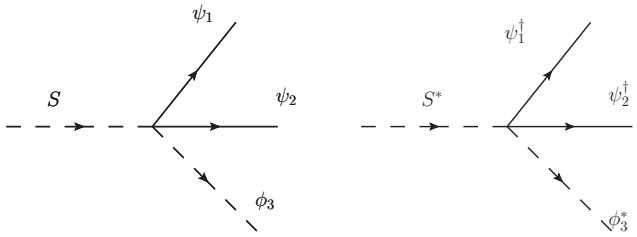

FIG. 5: The DM S three-body decays into the Higgs bosons and leptons, or the sleptons, Higgsinos as well as leptons.

state spin summed over

$$|i\mathcal{M}|^2 = 4\mathcal{C}^2\mathcal{C}_I^2(p_1 \cdot p_2 + m_1 m_2) \ , \tag{A1}$$

where $\mathcal{C}$ is the coupling constant with mass dimension -1, and $\mathcal{C}_I$ is the possible mixing factor arising from converting the interaction state into the mass eigenstate. The mass m_1 is still kept in the momentum, and then will be set to zero finally.

Appendix B: Fragmentation Function

Fragmentation function dN/dx_I is analytically calculable for three-body decay $Y \to a + b + c$. For the isotropic decay it is very convenient [43] to write the phase space integral according to the scaled variables $x_I = 2P_I \cdot Y/\sqrt{Y^2}$, where the invariant mass is defined as $Y^2 = (a + b + c)^2$. Here, the particles and their four-momenta are labeled with the same symbols. In the rest frame of Y, we have $Y = m_Y$ and $x_I = 2E_I/m_Y$. The three-body phase

space is reduced to the two-body phase space by pairing a with b and further integrating over c

$$d_3(PS, Y \to abc) = \frac{Y^2}{128\pi^3} dx_a dx_b \ . \tag{B1}$$

Then we find that the spectrum of the observed final state, for instance a, is obtained by integrating over x_b. Kinematics constrains x_a to be in the region

$$2\epsilon_a \leqslant x_a \leqslant 1 + \left(\epsilon_a^2 - \epsilon_b^2 - \epsilon_c^2 - 2\epsilon_b\epsilon_c\right) = R_a^{max}, \tag{B2}$$

where $\epsilon_a^2 \equiv m_a^2/Y^2$. If all the final state masses are ignorable, the region is between 0 and 1. For fixed x_a, x_b is constrained within the region $[R_b^-, R_b^+]$

$$\begin{aligned} R_b^{\pm} =& \frac{1}{2}(1 - x_a + \epsilon_a^2)^{-1}[(2 - x_a)(1 + \epsilon_a^2 + \epsilon_b^2 - \epsilon_c^2 - x_a) \pm \sqrt{x_a^2 - 4\epsilon_a^2}\lambda^{\frac{1}{2}}\left(1 + \epsilon_a^2 - x_a, \epsilon_b^2, \epsilon_c^2\right)] \\ \approx& \frac{1}{2}\left((2 - x_a) \pm x_a\right), \end{aligned} \tag{B3}$$

where the approximation is valid for small mass limit $\epsilon_{a,b,c} \ll 1$, and the triangle function is defined as $\lambda(x, y, z) = x^2 + y^2 + z^2 - 2xy - 2xz - 2yz$.

The general process is $S \to \psi_1\psi_2\phi_3$ with amplitude given in Eq. (A1). In terms of x and ϵ, we can write the amplitude as follows

$$|\mathcal{M}|^2 = 2(\mathcal{C}\mathcal{C}_{\mathcal{I}})^2 Y^2 \left(1 + \epsilon_3^2 - (\epsilon_2 + \epsilon_1)^2 - x_3\right) \ , \tag{B4}$$

which is symmetric for the subscripts 1 and 2. The distribution function of the fermion ψ_1 is obtained by paring ψ_1 and ϕ_3, *i.e.*, setting $a = \psi_1$, $b = \phi_3$, $c = \psi_2$,

$$\begin{aligned} \frac{dN}{dx_1} =& \frac{2(\mathcal{C}\mathcal{C}_{\mathcal{I}})^2 Y^4}{256\pi^3 m_D} \times \mathcal{N} \int_{R_3^-(x_1)}^{R_3^+(x_1)} dx_3 \left(1 + \epsilon_3^2 - (\epsilon_2 + \epsilon_1)^2 - x_3\right) \\ =& \frac{2(\mathcal{C}\mathcal{C}_{\mathcal{I}})^2 Y^4}{256\pi^3 m_D} \mathcal{N} \left[1 + \epsilon_3^2 - (\epsilon_2 + \epsilon_1)^2 - \frac{1}{2}\left(R_3^+(x_1) + R_3^-(x_1)\right)\right] \\ & \times \left(R_3^+(x_1) - R_3^-(x_1)\right), \end{aligned} \tag{B5}$$

where $\mathcal{N} = 1/\Gamma$ is the normalization factor. In the massless limit, it is approximated to be a simple function x_1^2. So the fermion spectrum is very hard. The distribution of ψ_2 is got simply by replacing the subscript 1 by 2 in the above formula. Similarly, we get the distribution function of scalar ϕ_3 by choosing $a = \phi_3$, $b = \psi_1$, and $c = \psi_2$

$$\begin{aligned} \frac{dN}{dx_3} =& \frac{2(\mathcal{C}\mathcal{C}_{\mathcal{I}})^2 Y^4}{256\pi^3 m_D} \mathcal{N} \int_{R_1^-(x_3)}^{R_1^+(x_3)} dx_1 \left(1 + \epsilon_3^2 - (\epsilon_2 + \epsilon_1)^2 - x_3\right) \\ =& \frac{2(\mathcal{C}\mathcal{C}_{\mathcal{I}})^2 Y^4}{256\pi^3 m_D} \mathcal{N} \left(1 + \epsilon_3^2 - (\epsilon_2 + \epsilon_1)^2 - x_3\right)\left(R_1^+(x_3) - R_1^-(x_3)\right). \end{aligned} \tag{B6}$$

Its massless limit is simplified to be $dN/dx_3 \to (1-x_3)x_3$, so the scalar spectrum is softer than the fermion spectrum. Integrating over x_3, we get the decay rate

$$\Gamma_I \approx \frac{1}{128\pi^3}\frac{1}{m_D} \times (\mathcal{C}\mathcal{C}_{\mathcal{I}})^2 Y^4 \times R_{I,F} \ , \tag{B7}$$

where

$$R_{I,F} = \frac{1}{6}\left(1 + 9\epsilon_3^2 + 12\epsilon_3^2 \log\epsilon_3 + 12\epsilon_2\epsilon_3 - 3\epsilon_2^2\right) . \tag{B8}$$

In this approximation, the terms involving ϵ_1 is negligible here. Furthermore, if ϵ_2 is also small enough, the last two terms can be discarded.

For convenience, we define the DM effective decay rate for all channels as the typical scale of its decay

$$\Gamma_{eff} \equiv \frac{1}{128\pi^3}\frac{1}{m_D} \times \mathcal{C}^2 Y^4 \ . \tag{B9}$$

Then we have $\Gamma_I = \Gamma_{eff}\mathcal{C}_I^2 R_{I,F}$. And the normalized distribution function is rewritten as a clear form $dN/dx = 1/R_{I,F} \times (d\widetilde{N}/dx)$.

1. General Cascade Decay Spectra

In our models, $e^{\pm}$ signals come from both the DM cascade decay and direct decay, for example,

$$S \to \widetilde{N}_{1,2}\mu\widetilde{\mu}, \quad \mu \to e\nu\nu, \quad \widetilde{\mu} \to \widetilde{N}_1 e. \tag{B10}$$

The positron energy spectrum in rest frame of S is determined to be the convolution of two distribution functions. Physically speaking, the fragmentation functions of the (N)MSSM particles (I, F) can be extracted out from PYTHIA [38]

$$\frac{dN}{dx_e^{I,F}}, \quad x_e^{I,F} \equiv \frac{2E_e^{I,F}}{m_{I,F}}, \tag{B11}$$

which is calculated in the rest frame of (I, F) particle. Converting to the rest frame of S, we obtain the total positron energy spectrum

$$\begin{aligned}\frac{dN}{dx_e^S} = &\sum_{I,F} B_{I,F} \int_{2\epsilon_{I,F}}^{R_{I,F}^{max}} dx_{I,F} \frac{1}{R_{I,F}} \frac{d\widetilde{N}}{dx_{I,F}} \int_{-1}^{1} d\cos\theta_{I,F} \int_{2\epsilon_e}^{\mathcal{I}_e} dx_e^I \frac{dN}{dx_e^{I,F}} \\ &\times \delta\left(2x_e^S x_{I,F}^{-1} - x_e^{I,F} - \cos\theta_{I,F}\sqrt{(x_e^{I,F})^2 - 4\epsilon_e^2}\sqrt{1-4\epsilon_{I,F}^2}\right),\end{aligned} \tag{B12}$$

with the scaled energies $x_e^S \equiv 2E_e^S/m_D$ and $x_{I,F} \equiv 2E_{I,F}/m_D$, and the mass ratios $\epsilon_e \equiv m_e/m_I$ and $\epsilon_{I,F} \equiv m_{I,F}/m_D$. The branch ratio $B_{I,F}$ is given by $B_{I,F} = \Gamma_{I,F}/\Gamma_{total}$. Notice that $\mathcal{I}_e$ denotes the largest positron energy fraction in the fragmentation of the (I, F)

particle. But the positron production is not clear in the course of fragmentation, so we cannot make sure the value of $\mathcal{I}_e$. However, for $m_e \ll m_{I,F}$, we have $\mathcal{I}_e = 1$ [44].

For three-body decays, the upper limit $R_{I,F}^{max}$ can be found in Eq. (B2). In the rest frame of the (I,F) particle, $\theta_{I,F}$ is the angle between the electron spatial momentum direction and the boost axis of the (I,F) particle. The $\delta-$function simply indicates that for some fixed boosted energy x_e^S, one should integrate over all possible configurations for $(x_e^{I,F}, \cos\theta_{I,F})$. In other words, Eq. (B12) makes the Lorentze boost of the energy spectrum: $dN/dx_e^{I,F} \to d\widetilde{N}/dx_e^S$, and then convoluted by the distribution $dN/dx_{I,F}$ that denotes the differential probability of S decay to (I,F) particle in the rest frame of S. Finally, we get the total positron energy spectrum.

For isotropic decay of the (I,F) particle, the distribution function is independent on angle, which can be integrated out

$$\begin{aligned}\frac{dN}{dx_e^S} =& \frac{\Gamma_{eff}}{\Gamma_{total}} \sum_{I,F} \frac{\mathcal{C}_{I,F}^2 R_{I,F}}{\sqrt{1-4\epsilon_{I,F}^2}} \int_{2\epsilon_{I,F}}^{R_{I,F}^{max}} dx_{I,F} \frac{1}{R_{I,F}} \frac{d\widetilde{N}}{dx_{I,F}} \int_{min(x_{I,F})}^{max(x_{I,F})} dx_e^{I,F} \\ & \frac{1}{\sqrt{(x_e^{I,F})^2 - 4\epsilon_e^2}} \frac{dN}{dx_e^{I,F}}. \end{aligned} \tag{B13}$$

The normalization condition of dN/dx_e^S in each decay channel is

$$\int \frac{dN}{dx_e^S} dx_e^S = multi_{I,F} \ , \tag{B14}$$

where $multi_{I,F}$ denotes how many electrons are produced by the fragmentation of each (I,F) particle. The integrand region in Eq. (B13) is given by $\min(x_{I,F}) = \mathcal{R}_-(x_{I,F})$ and $\max(x_{I,F}) = \min(\mathcal{I}_e, \mathcal{R}_+)$ with

$$\mathcal{R}_\pm(x_{I,F}) = \frac{1}{2}\left(x_e^S \pm \sqrt{1-4\epsilon_{I,F}^2} \sqrt{(x_e^S)^2 - 4(\epsilon_e \epsilon_{I,F} x_{I,F})^2} \right) \epsilon_{I,F}^{-2} x_{I,F}^{-1}. \tag{B15}$$

If $\mathcal{R}_- > \mathcal{I}_e$, the integral is zero. Then the constrained $\mathcal{R}_\pm$, which depends only on the ratio $r = x_e^S/x_{I,F}$, in turn constrains the integral region for $x_{I,F}$. If $\epsilon_{I,F} \ll 1$ is satisfied, then $R_+ \approx x_e^S/(x_I \epsilon_I^2) \gg 1$. So the upper limit always takes $\mathcal{I}_e$. For example, let us choose $(I,F) = \mu$. But in this paper, this is not always true since the sparticles and Higgs bosons are heavy. Consequently there are some values of r which gives $\mathcal{R}_+ > \mathcal{I}_e$. For the later case, one can show that $\mathcal{R}_\pm$ is monotonically increase with r, and the lower limit smaller than $\mathcal{I}_e$ gives the upper bound for $r \le \eta_2$, which is the larger root of $\mathcal{R}_- = 0$. However, in the former case, $\mathcal{R}_- > \mathcal{I}_e$ gives bound $\eta_1 \le r \le \eta_2$. In both cases, for fixed x_e^S, we must have $x_I \ge x_e^S/\eta_2$.

2. Analytical $e^{\pm}$ Spectra from Three-Body Cascade Decays

As an application, we use the above formulae to calculate the $e^{\pm}$ spectrum functions from $S \to \mu + fermion + scalar$ followed by μ three-body decay. Notice that $\epsilon_\mu \ll \epsilon_e \ll 1$ and $\eta_1 \leq r \leq \eta_2$, we obtain $2\eta_1\epsilon_\mu \leq x_e^S \leq R_\mu^{max}\eta_2$. The spectrum functions dN/dx_e^μ and $d\widetilde{N}/dx_\mu$ are respectively given by

$$\frac{dN}{dx_e^\mu} = 2(x_e^\mu)^2(3-2x_e^\mu), \qquad \frac{d\widetilde{N}}{dx_\mu} \approx \left(\frac{1}{2} - \frac{\epsilon_I^2}{1-x_\mu}\right) x_\mu^2 \,, \tag{B16}$$

where the approximated spectrum is calculated according to Eq. (B5).

If we are only interested in the positrons with energy higher than 1 GeV, we obtain $\mathcal{R}_- \approx x_e^S/x_\mu$. Integrating over x_e^μ and x_μ, we have

$$\begin{aligned}
\frac{dN}{dx_e^S} &= \int_{x_e^S/\eta_2}^{R_\mu^{max}} dx_\mu \left[\frac{5}{3} - 3\left(\frac{x_e^S}{x_\mu}\right)^2 + \frac{4}{3}\left(\frac{x_e^S}{x_\mu}\right)^3\right] \times \left(\frac{1}{2} - \frac{\epsilon_I^2}{1-x_\mu}\right) x_\mu^2 \\
&\approx \frac{5}{18} - \frac{3}{2}\left(x_e^S\right)^2 + \frac{11}{9}\left(x_e^S\right)^3 - \frac{2}{3}\left(x_e^S\right)^3 \log x_e^S \\
&+ \frac{\epsilon_I^2}{3}\left[5 - 5x_e^S + 2\left(x_e^S\right)^2 - 2\left(x_e^S\right)^3 + 4\left(x_e^S\right)^3 \log x_e^S \right. \\
&\left. +2\left(5 - 9\left(x_e^S\right)^2 + 4\left(x_e^S\right)^3\right)\right].
\end{aligned} \tag{B17}$$

The correction term is complicated but important since without it we cannot have the right order. This expression is valid for the energy fraction $2\epsilon_\mu\eta_2 \leq x_e^S \leq \eta_2 R_\mu^{max}$. The DM three-body cascade decay produces a harder spectrum than the two-body decay since its intermediate particle produces a hard spectrum. This is clearly shown in the muon case.

Appendix C: Fitting Positron Spectra

In this Appendix, we present the positron spectra got through the above procedure. Similarly, we can calculate the anti-proton spectra, although we will not present the details here. The basic method is to simulate the positron and anti-proton spectra in the rest frame of the sparticles and Higgs bosons via PYTHIA (each state (I, F) must be simulated separately and then summed over). We will not pay much attention to the detail fitting but present the results directly. Notation is consistent with the one given above, but we change the variable to energy, as in the original form from simulation.

The spectra are divided into three types: the type of sleptons, the type of Higgs bosons and the type of Higgsinos. For sleptons, the spectra from the left- and right-handed sparticles

have quite different behaviours, since their weak boson decays are different. The total $e^{\pm}$ from fragmentations are described by the following functions

$$\begin{aligned}
\widetilde{\mu}_L: &\quad \frac{dN}{dE} = \exp^{16.926-15.601E^{0.183}}\, E^{1.438}\left[1+14.90\log(1+0.05E)^{6.1}\right] - 8.5\times10^{-5}E^{0.55},\\
\widetilde{\nu}_{\mu L}: &\quad \frac{dN}{dE} = \exp^{16.913-15.601E^{0.183}}\, E^{1.437}\left[1+14.9\log(1+0.055E)^{6.5}\right] - 9.0\times10^{-7}E^{0.60},\\
\widetilde{\mu}_R: &\quad \frac{dN}{dE} = \frac{E^{1.302}}{0.245+262.353E^{1.971}} + \frac{E^{0.031}}{104.334+5.757\times10^{-5}E^{3.242}}\ .
\end{aligned} \tag{C1}$$

The type for all the Higgs bosons have the similar form, probably because they all are dominated by the H_d components. For simplicity, we only present A_0 as follows

$$A^0: \quad \frac{dN}{dE} = \exp^{17.716-15.601E^{0.160}}\, E^{1.327}\left[1+4.0\log(1+0.021E)^{3.0}\right] - 1.0\times10^{-6}E^{0.8}. \tag{C2}$$

At last, the fitting functions for the neutralinos $\widetilde{C}^0_{3,4}$ and charginos $\widetilde{C}^{\pm}_{1,2}$ are given by

$$\begin{aligned}
\widetilde{C}^0_3: &\quad \frac{dN}{dE} = \exp^{15.461-15.601E^{0.163}}\, E^{1.311}\left[1+40.0\log(1+0.025E)^{2.4}\right] - 2.7\times10^{-5}E^{0.7},\\
\widetilde{C}^0_4: &\quad \frac{dN}{dE} = \exp^{17.880-15.601E^{0.174}}\, E^{1.408}\left[1+14.0\log(1+0.024E)^{4.2}\right] - 1.7\times10^{-6}E^{0.5},\\
\widetilde{C}^{\pm}_1: &\quad \frac{dN}{dE} = \exp^{17.198-15.601E^{0.195}}\, E^{1.494}\left[1-1.1\log(1+0.045E)^{3.0}\right] - 2.7\times10^{-6}E^{0.5},\\
\widetilde{C}^{\pm}_2: &\quad \frac{dN}{dE} = \exp^{17.814-15.601E^{0.174}}\, E^{1.416}\left[1+13.0\log(1+0.026E)^{3.5}\right] + 1.4\times10^{-6}E^{1.4}\ .
\end{aligned} \tag{C3}$$

Basically, these fitting functions consist of three parts. The first part describes the low

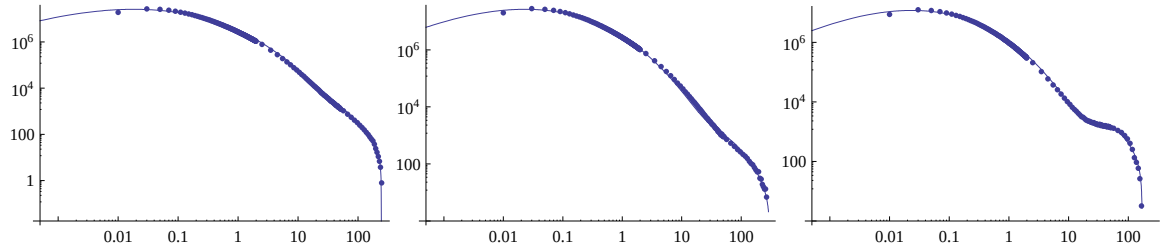

FIG. 6: Typical fitting functions: $\widetilde{C}^0_4$ (left), H (middle) and $\widetilde{\mu}_L$ (right). In the simulations, 3×10^5 events have been generated by PYTHIA.

energy region very well, the second logarithmic part is added to slow down the exceptional decreasing, and the last part is used to modulate the region near the DM mass cutoff region. This kind of fitting functions is not universal, and only applies to our parameter sets. We

present the typical fittings for three types in Fig. 6. By the way, the small discrepancies between the fitting functions and simulations do exist at high energy. So the fitting functions are simply used as the referred fitting functions.

---

[1] J. Chang *et al.*, Nature **456**, 362 (2008).

[2] S. Torii *et al.* [PPB-BETS Collaboration], arXiv:0809.0760 [astro-ph].

[3] O. Adriani *et al.* [PAMELA Collaboration], Nature **458**, 607 (2009).

[4] O. Adriani *et al.*, Phys. Rev. Lett. **102**, 051101 (2009).

[5] A. A. Abdo *et al.* [The Fermi LAT Collaboration], Phys. Rev. Lett. **102**, 181101 (2009).

[6] H. E. S. S. Collaboration, arXiv:0905.0105 [astro-ph.HE].

[7] F. Aharonian *et al.* [H.E.S.S. Collaboration], Phys. Rev. Lett. **101**, 261104 (2008).

[8] J. Lavalle, Q. Yuan, D. Maurin and X. J. Bi, arXiv:0709.3634 [astro-ph].

[9] J. Hisano, S. Matsumoto and M. M. Nojiri, Phys. Rev. Lett. **92**, 031303 (2004); M. Cirelli, R. Franceschini and A. Strumia, Nucl. Phys. B **800**, 204 (2008).

[10] N. Arkani-Hamed, D. P. Finkbeiner, T. R. Slatyer and N. Weiner, Phys. Rev. D **79**, 015014 (2009).

[11] Y. Nomura and J. Thaler, Phys. Rev. D **79**, 075008 (2009).

[12] D. Feldman, Z. Liu and P. Nath, Phys. Rev. D **79**, 063509 (2009); M. Ibe, H. Murayama and T. T. Yanagida, Phys. Rev. D **79**, 095009 (2009); W. L. Guo and Y. L. Wu, Phys. Rev. D **79**, 055012 (2009); X. J. Bi, X. G. He and Q. Yuan, Phys. Lett. **B678**, 168 (2009).

[13] X. J. Bi, R. Brandenberger, P. Gondolo, T. Li, Q. Yuan and X. m. Zhang, Phys. Rev. D **80**, 103502 (2009).

[14] C. R. Chen and F. Takahashi, JCAP **0902**, 004 (2009).

[15] P. f. Yin, Q. Yuan, J. Liu, J. Zhang, X. j. Bi and S. h. Zhu, Phys. Rev. D **79**, 023512 (2009).

[16] A. Arvanitaki, S. Dimopoulos, S. Dubovsky, P. W. Graham, R. Harnik and S. Rajendran, Phys. Rev. D **79**, 105022 (2009).

[17] A. Ibarra, D. Tran and C. Weniger, arXiv:0906.1571 [hep-ph].

[18] E. Nardi, F. Sannino and A. Strumia, JCAP **0901**, 043 (2009); J. T. Ruderman and T. Volansky, arXiv:0907.4373 [hep-ph]; A. Ibarra and D. Tran, JCAP **0902**, 021 (2009); M. Luo, L. Wang, W. Wu and G. Zhu, arXiv:0911.3235 [hep-ph].

[19] J. Liu, Q. Yuan, X. Bi, H. Li and X. Zhang, arXiv:0906.3858 [astro-ph.CO].

[20] Z. Ahmed *et al.* [The CDMS-II Collaboration], arXiv:0912.3592 [astro-ph.CO].

[21] M. Kadastik, K. Kannike, A. Racioppi and M. Raidal, arXiv:0912.2729 [hep-ph]; M. Kadastik, K. Kannike, A. Racioppi and M. Raidal, arXiv:0912.3797 [hep-ph]; N. Bernal and A. Goudelis, arXiv:0912.3905 [hep-ph]; A. Bottino, F. Donato, N. Fornengo and S. Scopel, arXiv:0912.4025 [hep-ph]; D. Feldman, Z. Liu and P. Nath, arXiv:0912.4217 [hep-ph]; J. Kopp, T. Schwetz and J. Zupan, arXiv:0912.4264 [hep-ph]; R. Allahverdi, B. Dutta and Y. Santoso, arXiv:0912.4329 [hep-ph]; M. Endo, S. Shirai and K. Yonekura, arXiv:0912.4484 [hep-ph]; M. Holmes and B. D. Nelson, arXiv:0912.4507 [hep-ph]; Q. H. Cao, C. R. Chen, C. S. Li and H. Zhang, arXiv:0912.4511 [hep-ph]; K. Cheung and T. C. Yuan, arXiv:0912.4599 [hep-ph]; J. Hisano, K. Nakayama and M. Yamanaka, arXiv:0912.4701 [hep-ph]; X. G. He, T. Li, X. Q. Li, J. Tandean and H. C. Tsai, arXiv:0912.4722 [hep-ph]; M. Asano and R. Kitano, arXiv:1001.0486 [hep-ph]; I. Gogoladze, R. Khalid, S. Raza and Q. Shafi, arXiv:0912.5411 [hep-ph]; M. Aoki, S. Kanemura and O. Seto, arXiv:0912.5536 [hep-ph]; R. Foot, arXiv:1001.0096 [hep-ph]; W. L. Guo, Y. L. Wu and Y. F. Zhou, arXiv:1001.0307 [hep-ph]; J. Shu, P. f. Yin and S. h. Zhu, arXiv:1001.1076 [hep-ph].

[22] C. Boehm, P. Fayet and J. Silk, Phys. Rev. D **69**, 101302 (2004); E. Ma, Annales Fond. Broglie **31**, 285 (2006); Q. H. Cao, E. Ma, J. Wudka and C. P. Yuan, arXiv:0711.3881 [hep-ph]; M. Adibzadeh and P. Q. Hung, Nucl. Phys. B **804**, 223 (2008); J. L. Feng and J. Kumar, Phys. Rev. Lett. **101**, 231301 (2008); H. Sung Cheon, S. K. Kang and C. S. Kim, Phys. Lett. B **675**, 203 (2009); J. H. Huh, J. E. Kim and B. Kyae, Phys. Rev. D **79**, 063529 (2009); M. Fairbairn and J. Zupan, JCAP **0907**, 001 (2009),[Published Version]; K. M. Zurek, Phys. Rev. D **79**, 115002 (2009); B. Batell, M. Pospelov and A. Ritz, Phys. Rev. D **79**, 115019 (2009); S. Profumo, K. Sigurdson and L. Ubaldi, JCAP **0912**, 016 (2009); F. Chen, J. M. Cline and A. R. Frey, Phys. Rev. D **80**, 083516 (2009); H. Zhang, C. S. Li, Q. H. Cao and Z. Li, arXiv:0910.2831 [hep-ph].

[23] T. Hur, H. S. Lee and S. Nasri, Phys. Rev. D **77**, 015008 (2008).

[24] C. D. Froggatt and H. B. Nielsen, Nucl. Phys. B **147**, 277 (1979).

[25] M. B. Green and J. H. Schwarz, Phys. Lett. B **149**, 117 (1984).

[26] L. E. Ibanez and G. G. Ross, Phys. Lett. B **332**, 100 (1994); V. Jain and R. Shrock, Phys. Lett. B **352**, 83 (1995); E. Dudas, S. Pokorski and C. A. Savoy, Phys. Lett. B **356**, 45 (1995); P. Binetruy, S. Lavignac and P. Ramond, Nucl. Phys. B **477**, 353 (1996); N. Irges, S. Lavignac and P. Ramond, Phys. Rev. D **58**, 035003 (1998); N. Maekawa, Prog. Theor. Phys. **106**, 401 (2001).

[27] H. K. Dreiner, H. Murayama and M. Thormeier, Nucl. Phys. B **729**, 278 (2005).

[28] R. Harnik, D. T. Larson, H. Murayama and M. Thormeier, Nucl. Phys. B **706**, 372 (2005); H. K. Dreiner, C. Luhn, H. Murayama and M. Thormeier, Nucl. Phys. B **774**, 127 (2007);

Nucl. Phys. B **795**, 172 (2008).

[29] I. Gogoladze, C. A. Lee, T. Li and Q. Shafi, Phys. Rev. D **78**, 015024 (2008).

[30] L. E. Ibanez and G. G. Ross, Phys. Lett. B **260** (1991) 291; Nucl. Phys. B **368**, 3 (1992).

[31] H. K. Dreiner, C. Luhn and M. Thormeier, Phys. Rev. D **73**, 075007 (2006).

[32] M. Cvetic, D. A. Demir, J. R. Espinosa, L. L. Everett and P. Langacker, Phys. Rev. D **56**, 2861 (1997) [Erratum-ibid. D **58**, 119905 (1998)]. P. Langacker and J. Wang, Phys. Rev. D **58**, 115010 (1998).

[33] H. S. Lee, Phys. Lett. B **663**, 255 (2008).

[34] J. Edsjo and P. Gondolo, Phys. Rev. D **56**, 1879 (1997); I. Niessen, arXiv:0809.1748 [hep-ph].

[35] G. Belanger, F. Boudjema, A. Pukhov and A. Semenov, Comput. Phys. Commun. **176**, 367 (2007).

[36] A. Djouadi, J. L. Kneur and G. Moultaka, Comput. Phys. Commun. **176**, 426 (2007).

[37] J. F. Navarro, C. S. Frenk and S. D. M. White, Astrophys. J. **490**, 493 (1997).

[38] T. Sjostrand, S. Mrenna and P. Skands, JHEP **0605**, 026 (2006).

[39] T. Delahaye, R. Lineros, F. Donato, N. Fornengo and P. Salati, Phys. Rev. D **77**, 063527 (2008).

[40] E. A. Baltz and J. Edsjo, Phys. Rev. D **59**, 023511 (1998).

[41] D. Maurin, F. Donato, R. Taillet and P. Salati, Astrophys. J. **555**, 585 (2001); J. Hisano, S. Matsumoto, O. Saito and M. Senami, Phys. Rev. D **73**, 055004 (2006).

[42] P. Meade, M. Papucci, A. Strumia and T. Volansky, arXiv:0905.0480 [hep-ph].

[43] V. Barger and R. J. N. Phillips, "Collider Physics", 1996.

[44] If $(I, F) = \mu$, the positron energy fraction from the muon three-body decay indeed has the upper limit about 1 from Eq. (B2). However, the positrons from the slepton or Higgs boson fragmentations tend to have a much softer spectrum. The PYTHIA simulation confirms this point.